Toward the Speed Limit of High-Fidelity Two-Qubit Gates

Swathi S. Hegde,[*,§] Jingfu Zhang,[†] and Dieter Suter[‡]
Fakultät Physik, Technische Universität Dortmund, D-44221 Dortmund, Germany

(Received 10 February 2022; accepted 4 May 2022; published 8 June 2022)

Most implementations of quantum gate operations rely on external control fields to drive the evolution of the quantum system. Generating these control fields requires significant efforts to design the suitable control Hamiltonians. Furthermore, any error in the control fields reduces the fidelity of the implemented control operation with respect to the ideal target operation. Achieving sufficiently fast gate operations at low error rates remains therefore a huge challenge. In this Letter, we present a novel approach to overcome this challenge by eliminating, for specific gate operations, the time-dependent control fields entirely. This approach appears useful for maximizing the speed of the gate operation while simultaneously eliminating relevant sources of errors. We present an experimental demonstration of the concept in a single nitrogen-vacancy center in diamond at room temperature.

DOI: 10.1103/PhysRevLett.128.230502

Introduction.—Quantum gates are the elementary steps for processing quantum information. They are therefore essential for all quantum technologies, such as quantum computing [1–3] or quantum sensing [4–6], and they must be implemented in all types of quantum registers such as superconducting qubit systems [7,8], ion traps [9,10], or hybrid qubit systems, combining, e.g., electronic and nuclear spins [4–6]. In most cases, elementary quantum gates are realized by segments of external control fields, often including free evolution periods [11–15]. Designing these sequences of control fields is an optimization task, where the number of control field segments, their strengths, durations, and phases are adjusted such that the resulting unitary has maximum overlap with the target quantum gate [16–19]. The duration of the gates is limited by the strength of the couplings between the qubits and by the strength of the interaction between the qubits and the control fields [20–22].

These limitations become severe when gate operation times exceed the qubit coherence times, and thus coherent control becomes impossible. Although various techniques were demonstrated for alleviating this problem like protected quantum gates [23,24] or indirect control [17,25], they add control overhead, and the resulting gate durations still tend to be long. Here, we introduce a novel approach to overcome these challenges, which results in highly efficient gates that have the shortest possible durations without any control overhead.

The computational basis states of a single qubit are $|0\rangle$ and $|1\rangle$, and for a two-qubit system $\{|00\rangle, |01\rangle, |10\rangle, |11\rangle\}$. While the computational basis states are usually assigned to eigenstates of the Hamiltonian, we choose here a different approach where some computational states are not eigenstates of the system Hamiltonian. This allows us to generate logical operations such as a conditional rotation (CR) without applying control fields, simply by allowing the system to evolve under its internal Hamiltonian. In the example discussed below, the states $|00\rangle$ and $|01\rangle$ are eigenstates of the system Hamiltonian and hence do not evolve, while $|10\rangle$ and $|11\rangle$ are superpositions of eigenstates. The evolution of this system therefore generates a conditional gate operation with the first qubit acting as the control qubit. The evolution is periodic, with period $t_p = 2\pi/|\mathcal{E}_3 - \mathcal{E}_4|$, where $\mathcal{E}_i$ are the energies of the eigenstates, and we choose units where $\hbar = 1$. Thus for a delay τ, the free evolution implements a conditional rotation $U_{\mathrm{CR}}(\alpha)$ with the rotation angle $\alpha = 2\pi\tau/t_p = \tau|\mathcal{E}_3 - \mathcal{E}_4|$, such that $U_{\mathrm{CR}}(\alpha)$ reaches the quantum speed limit given by the energy of the system [12,20,21]. The resulting $U_{\mathrm{CR}}(\alpha)$ is the fastest possible gate for the given Hamiltonian and is not affected by errors in control fields. In this Letter, we provide details on how this type of gate operations can be implemented and show experimental results.

Hamiltonian and computational basis.—For the demonstration of this fast gate operation, we use a single nitrogen-vacancy (NV) center in diamond at room temperature [26–30]. The NV center consists of a spin-1 electron coupled to a spin-1 ^{14}N and a spin-1/2 ^{13}C, as shown in Fig. 1(a). For the two-qubit operation, we choose a subsystem consisting of two of the electron spin levels as the control qubit and the ^{13}C spin as the target qubit, while the ^{14}N is a passive spin that is not affected by the gate operations. The secular part of the electron-^{13}C system Hamiltonian in the laboratory frame is

$$\frac{\mathcal{H}}{2\pi} = DS_z^2 - \nu_e S_z - \nu_C I_z + A_{zz} S_z I_z + A_{zx} S_z I_x, \quad (1)$$

where S_z and $I_{z/x}$ are the spin operators for the electron and the ^{13}C, respectively, $D = 2.870$ GHz is the zero field

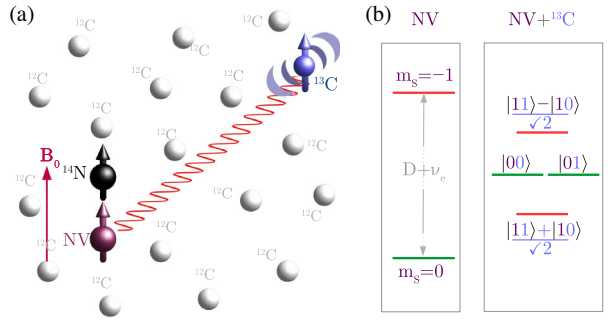

FIG. 1. (a) Structure of the NV system consisting of an electron and two nuclear spins: ^{14}N and ^{13}C. The magnetic field is oriented along the NV axis which we take to be the z axis. The ^{13}C atom is at a distance of 0.89 nm from the electron and hence is weakly coupled. The other nuclei are spinless ^{12}C. (b) Energy levels of the electron (left) and system subspace consisting of two electron spin states and the ^{13}C.

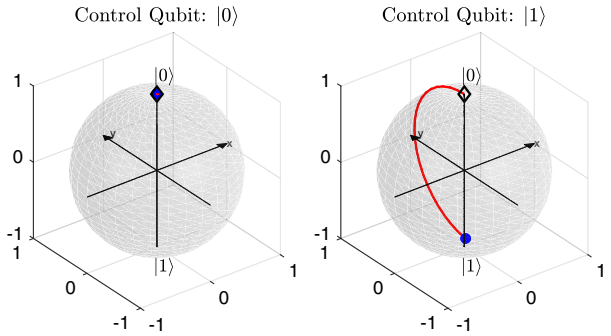

FIG. 2. Bloch sphere representation of the evolution of the ^{13}C spin initially in state $|0\rangle$, when the electron spin is in $|0\rangle$ (left) and $|1\rangle$ (right), during $U_{\mathrm{CR}}(\pi)$. The black diamonds and blue circles indicate the initial and the final states respectively.

splitting of the electron, $A_{zz} = -0.152$ MHz and $A_{zx} = 0.110$ MHz are the longitudinal and transverse components of the hyperfine coupling with ^{13}C, $\nu_e = (\gamma_e B_0 - 2.16)$ MHz $= -400.110$ MHz is the electron Larmor frequency that includes the shift from the ^{14}N hyperfine coupling when the nitrogen is in the $m_N = 1$ state, and $\nu_C = \gamma_C B_0 = 0.152$ MHz is the ^{13}C Larmor frequency in a magnetic field $B_0 = 14.2$ mT. Here γ_e and γ_C are the gyromagnetic ratios of electron and ^{13}C, respectively.

In the presence of B_0, the two transitions between the electron spin states $m_S = 0 \leftrightarrow -1$ and $0 \leftrightarrow +1$ are well separated with a frequency difference of $2\nu_e$. We choose to implement our gates in the electron subspace $m_S = \{0, -1\}$ and define s_z as the pseudospin-1/2 operator for this subspace, with eigenvalues $\pm 1/2$. Each of the two electron spin levels splits into two due to the coupling with ^{13}C. The resulting four levels form our system subspace, and we call its Hamiltonian the subspace Hamiltonian $\mathcal{H}_s$ (see the Supplemental Material [31]). We choose the eigenstates of s_z and I_z as the computational basis states $\{|0\rangle, |1\rangle\} \otimes \{|0\rangle, |1\rangle\}$.

We transform the subspace Hamiltonian to an interaction frame as

$$\begin{aligned}\mathcal{H}_I &= \mathcal{U}_{\mathrm{tr}}(\tau)\mathcal{H}_s\mathcal{U}_{\mathrm{tr}}^{\dagger}(\tau) - i\mathcal{U}_{\mathrm{tr}}(\tau)\frac{d\mathcal{U}_{\mathrm{tr}}^{\dagger}(\tau)}{d\tau} \\ &= |1\rangle\langle 1| \otimes [-2\pi A_{zx} I_x], \end{aligned} \tag{2}$$

where the interaction frame is defined by the unitary $\mathcal{U}_{\mathrm{tr}}(\tau) = \exp(-i2\pi\tau[\nu_C|0\rangle\langle 0| \otimes I_z + (D+\nu_e)s_z \otimes I - ((D+\nu_e)/2) \times I \otimes I])$, where I is the 2×2 identity operator (see the Supplemental Material [31]). The energy eigenstates of $\mathcal{H}_I$ are $\{|00\rangle, |01\rangle, |1\psi\rangle, |1\phi\rangle\}$, where $|\psi\rangle = (|1\rangle + |0\rangle/\sqrt{2})$ and $|\phi\rangle = (|1\rangle - |0\rangle/\sqrt{2})$, with eigenvalues $\mathcal{E}_1 = \mathcal{E}_2 = 0$ and $\mathcal{E}_3 = -\mathcal{E}_4 = \pi A_{zx}$, as indicated in Fig. 1(b).

With this Hamiltonian, a free evolution of duration τ generates the propagator

$$U_{\mathrm{CR}}(\alpha) = \exp(-i\mathcal{H}_I\tau) = |0\rangle\langle 0| \otimes I + |1\rangle\langle 1| \otimes R_x(\alpha), \tag{3}$$

where $R_x(\alpha) = \exp(i\alpha I_x)$. This corresponds, as intended, to a controlled rotation gate: if the control qubit (the electron) is in state $|0\rangle$, the target qubit (the nuclear spin) does not evolve; if the control qubit is in state $|1\rangle$, the target qubit is rotated around the x axis.

The speed of a logical gate is limited by the average energy of the quantum system [12,20,21]. The difference between the energies of the eigenstates in the $m_S = -1$ subspace is $2\pi A_{zx}$ and thus for the controlled rotation gate $U_{\mathrm{CR}}(\alpha)$, the minimum gate time is $\tau = \alpha/2\pi|A_{zx}|$. In our system, where $A_{zx} = 0.110$ MHz, a free evolution time of $\tau = 4.545$ μs corresponds to $\alpha = \pi$ and reaches the quantum speed limit. Figure 2 shows the evolution trajectory of the ^{13}C spin on the Bloch sphere when it is initially in $|0\rangle$. If the electron is in state $|0\rangle$, the nuclear spin does not evolve. If it is in $|1\rangle$, the nuclear spin evolves from $|0\rangle \rightarrow |1\rangle$ along a great circle trajectory, indicating this is the fastest possible gate for the given system.

Experimental demonstration.—In our experiment we apply the delay-only $U_{\mathrm{CR}}(\alpha)$ to the states $|00\rangle$ and $|10\rangle$ to check its effect when the control qubit is in the state $|0\rangle$ and $|1\rangle$, respectively. After the $U_{\mathrm{CR}}(\alpha)$ operation, we measure the diagonal elements of the final density operator in the computational basis [32].

The preparation of the initial state $|00\rangle$ from the maximally mixed state of the spin system is as follows: a 532 nm wavelength laser pulse of duration 5 μs and power $\approx$0.5 mW sets the electron to its ground state $|0\rangle$ while the ^{13}C spin remains in the maximally mixed state. We then swap the states of electron and ^{13}C spins before resetting the electron spin to the ground state using another laser pulse [16,25]. After the second laser pulse, the populations of the states $|00\rangle$ and $|01\rangle$ are 0.91 and

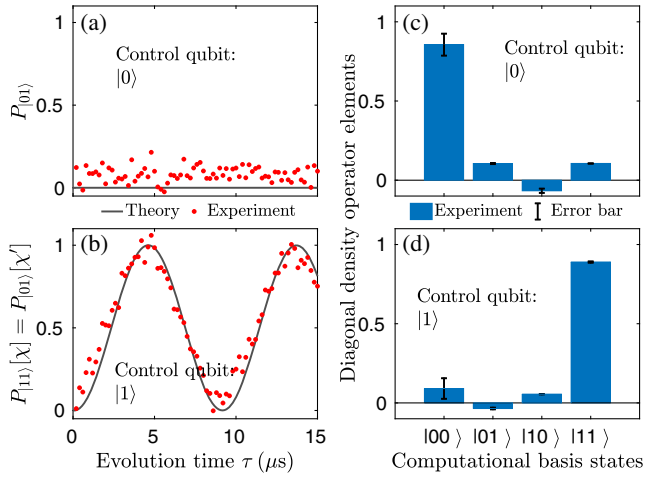

FIG. 3. Theoretical and experimental results to demonstrate the effect of $U_{\mathrm{CR}}(\alpha)$ using the delay-only sequence starting from the initial states $|00\rangle$ (top) and $|10\rangle$ (bottom). (a–b) The plots represent $P_{|01\rangle}$ (a) and $P_{|11\rangle}$ (b) as a function of the evolution time τ. $P_{|11\rangle}[\chi] = P_{|01\rangle}[\chi'] = [1-\cos(2\pi A_{zx}\tau)]/2$ oscillates from the initial value of 0 to a maximum of 1 after $\tau = 4.545$ μs, indicating the effect of $U_{\mathrm{CR}}(\pi)$. (c–d) Diagonal density operator elements of the final states in the computational basis.

0.09, respectively [25,32]. To further purify the state, we use a clean-up operation U_{cu} of the form $(90^{\circ}_{y} - d - 90^{\circ}_{x})$, which selectively removes the spurious population of $|01\rangle$ from our system subspace to $m_S = +1$ [33]. Here $90^{\circ}_{x/y}$ are MW pulses acting on the electron spin, with the carrier frequency set to the transition $m_S = 0 \leftrightarrow +1$, which rotate the electron spin by 90° around the x/y axis and $d = 1/2|A_{zz}|$ is the delay between the two $90^{\circ}_{x/y}$ pulses (see the Supplemental Material [31]). As a result only $|00\rangle$ remains populated in the computational subspace, and the system subspace is fully polarized. A similar MW pulse sequence with opposite pulse phases of the form $(90^{\circ}_{x} - d - 90^{\circ}_{y})$ selectively removes the population of $|00\rangle$ from the system subspace to $m_S = +1$ [32,33], and we call this different clean-up operation V_{cu} (see the Supplemental Material [31]). Below, we show how V_{cu} can be incorporated as a part of our readout process.

In the NV system, readout of the state of the system is performed by counting photons during a laser pulse. The resulting count rate is a measure of the population of the ground state $m_S = 0$; the signal therefore represents the sum of the two populations $P_{|00\rangle}$ and $P_{|01\rangle}$ in the states $|00\rangle$ and $|01\rangle$, respectively.

To check the effect of $U_{\mathrm{CR}}(\alpha)$ when the control qubit is in $|0\rangle$, we let the initial state $|00\rangle$ evolve under $\mathcal{H}_I$ for a variable duration $\tau = \alpha/2\pi|A_{zx}|$. We then implement another clean-up operation V_{cu}, and thus the population measured during the readout laser pulse corresponds to $P_{|01\rangle}$. In Fig. 3(a), we show the corresponding theoretical and experimental plots of $P_{|01\rangle}$ vs τ.

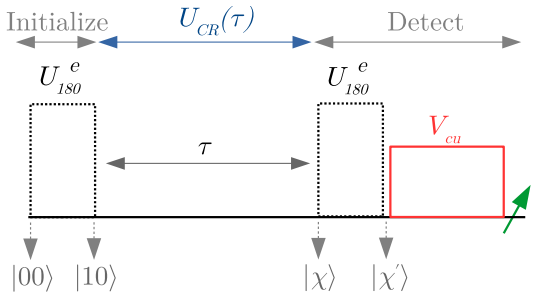

FIG. 4. Pulse sequence to check the effect of $U_{\mathrm{CR}}(\alpha)$ when the control qubit is in state $|1\rangle$.

We now check the effect of $U_{\mathrm{CR}}(\alpha)$ when the control qubit is in $|1\rangle$ by preparing the initial state $|10\rangle$, using the pulse sequence given in Fig. 4: starting from $|00\rangle$, we apply an operation $U^{e}_{180} = \exp(-i\pi s_x)$ as a MW pulse resonant with the transition $m_S = 0 \leftrightarrow -1$ with an amplitude of 7 MHz that rotates the electron spin by 180° and exchanges the states $|00\rangle \leftrightarrow |10\rangle$. During the subsequent delay τ, $|10\rangle$ evolves to $|\chi\rangle = \cos(\pi A_{zx}\tau)|10\rangle + i\sin(\pi A_{zx}\tau)|11\rangle$ under the Hamiltonian $\mathcal{H}_I$. The numerical simulation of the probability $P_{|11\rangle}(\tau) = [1-\cos(2\pi A_{zx}\tau)]/2$ of finding the system in $|11\rangle$ vs τ is shown in Fig. 3(b).

In order to measure $P_{|11\rangle}$, we apply another U^{e}_{180} operation to $|\chi\rangle$ to flip the electron states $m_S = -1 \leftrightarrow m_S = 0$ such that $|\chi'\rangle = U^{e}_{180}|\chi\rangle = \cos(\pi A_{zx}\tau)|00\rangle + i\sin(\pi A_{zx}\tau)|01\rangle$ followed by another clean-up operation V_{cu}. Since U^{e}_{180} flips $|11\rangle \leftrightarrow |01\rangle$, the measured signal represents $P_{|11\rangle}[\chi] = P_{|01\rangle}[\chi']$. The experimental results of $P_{|11\rangle}$ vs τ are shown in Fig. 3(b).

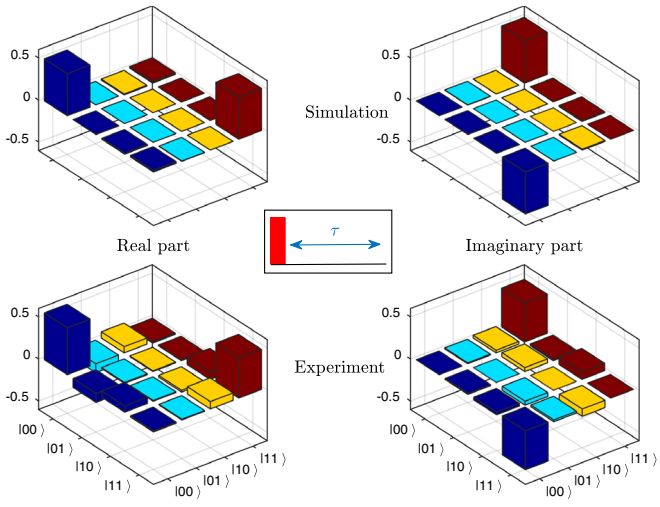

FIG. 5. Simulated (top trace) and experimental (bottom trace) density matrices of the Bell-type state $|\beta\rangle = (|00\rangle + i|11\rangle)/\sqrt{2}$, in the computational basis. The left column indicates the real part of the density matrix, and the right column indicates the imaginary part. Inset: the pulse sequence to generate this state: the solid rectangle indicates a 90° MW pulse on the electron with a phase of 270°, and the delay corresponds to $U_{\mathrm{CR}}(\pi)$.

We also measured the other diagonal elements of the final density operators using the procedure of Ref. [32]. The results shown in Figs. 3(c) and 3(d) verify that the state remains unchanged when the control qubit is in $|0\rangle$, and the target qubit is flipped when the control qubit is in $|1\rangle$. The experimental state fidelities are >0.98 and >0.99 for Figs. 3(c) and 3(d) respectively. The state fidelity is $F = (\mathrm{Tr}(\rho\rho_t)/\sqrt{\mathrm{Tr}(\rho^2)\mathrm{Tr}(\rho_t^2)})$, where ρ_t is the target state and ρ is the experimental final state.

Discussion.—A typical quantum sensing or computing protocol requires a combination of multiple gates. In such quantum circuits, integration of our $U_{\mathrm{CR}}(\alpha)$ with other gates that require active control fields is a necessity. In the typical case where two-qubit gates are speed limiting, efficient two-qubit gates like the one introduced here have a significant effect on the execution time of the full protocol. As an example, a Bell state can be prepared from an initial state $\psi_0 = |00\rangle$ by applying a Hadamard gate on the first qubit followed by a controlled NOT (CNOT) gate targeting the second qubit [11,12]. We here replace the Hadamard gate with the pseudo-Hadamard gate on the electron spin and implement the CNOT gate by the free evolution. The corresponding pulse sequence to prepare the Bell-type state is shown in the inset of Fig. 5. The solid rectangle is a 90° MW pulse that creates an equal superposition between the electron states $|0\rangle$ and $|1\rangle$. After a free evolution of duration $\tau = 4.545$ μs, the ideal Bell-type state is $|\beta\rangle = (|00\rangle + i|11\rangle)/\sqrt{2}$. The simulated density matrix $|\beta_s\rangle\langle\beta_s|$ obtained using the pulse sequence $(90° - \tau)$, where the duration of the initial 90° MW pulse is 0.125 μs, is shown in the upper trace of Fig. 5. Its state fidelity with $|\beta\rangle\langle\beta|$ is 99.9%. The reconstruction of the experimental final state using full state tomography [32] is shown in the lower trace of Fig. 5, and its state fidelity with $|\beta\rangle\langle\beta|$ is 96%. The experimental errors are mainly due to the uncertainty of ≈2% due to the readout gate operations required for quantum state tomography [32] and due to the photon counting statistics of ≈3%.

For multiqubit systems, the implementation of our fastest gates is limited by the spectral resolution [34]. In such cases, one can combine our gates with dynamical decoupling to extend the T_2^* [23]; this will be a subject of future work.

Conclusion.—In conclusion, we have introduced a highly efficient two-qubit gate operation that uses only free evolution under the static system Hamiltonian. Here, for a given Hamiltonian, we chose computational basis states that are not the eigenstates of the system Hamiltonian. Our scheme to implement the two-qubit gate does not contribute to the control overhead or to control errors. To demonstrate our scheme, we choose a quantum register consisting of a single ^{13}C spin coupled to the electron spin of a NV center in diamond. The two-qubit gate efficiency derives from the hyperfine coupling that is much stronger than the typical Rabi frequencies of the nuclear spins. Integration of our individual controlled rotation gates with gates that require active fields can improve the overall efficiency of the full quantum computing or quantum sensing protocols.

This project has received funding from the European Union's Horizon 2020 research and innovation program under Grant Agreement No. 828946. The publication reflects the opinion of the authors; the agency and the commission may not be held responsible for the information contained in it.

S. H. and J. Z. contributed equally to this work.

*swathi.hegde@tu-dortmund.de
†jingfu.zhang@tu-dortmund.de
‡Dieter.Suter@tu-dortmund.de
§Present address: Quantum Brilliance GmbH 5.0G, Industriestrasse 4, 70565 Stuttgart, Germany.

[1] P. W. Shor, SIAM Rev. **41**, 303 (1999).
[2] L. K. Grover, arXiv:quant-ph/9605043.
[3] I. M. Georgescu, S. Ashhab, and F. Nori, Rev. Mod. Phys. **86**, 153 (2014).
[4] C. Degen, Appl. Phys. Lett. **92**, 243111 (2008).
[5] J. Taylor, P. Cappellaro, L. Childress, L. Jiang, D. Budker, P. Hemmer, A. Yacoby, R. Walsworth, and M. Lukin, Nat. Phys. **4**, 810 (2008).
[6] C. L. Degen, F. Reinhard, and P. Cappellaro, Rev. Mod. Phys. **89**, 035002 (2017).
[7] M. H. Devoret and R. J. Schoelkopf, Science **339**, 1169 (2013).
[8] J. M. Chow, J. M. Gambetta, A. D. Corcoles, S. T. Merkel, J. A. Smolin, C. Rigetti, S. Poletto, G. A. Keefe, M. B. Rothwell, J. R. Rozen, M. B. Ketchen, and M. Steffen, Phys. Rev. Lett. **109**, 060501 (2012).
[9] D. Kielpinski, C. Monroe, and D. J. Wineland, Nature (London) **417**, 709 (2002).
[10] J. I. Cirac and P. Zoller, Phys. Rev. Lett. **74**, 4091 (1995).
[11] M. A. Nielsen and I. L. Chuang, *Quantum Computation and Quantum Information* (Cambridge University Press, Cambridge, England, 2002).
[12] J. Stolze and D. Suter, *Quantum Computing: A Short Course from Theory to Experiment* (John Wiley & Sons, New York, 2008).
[13] A. Daskin and S. Kais, J. Chem. Phys. **134**, 144112 (2011).
[14] D. P. DiVincenzo, Phys. Rev. A **51**, 1015 (1995).
[15] A. Barenco, D. Deutsch, A. Ekert, and R. Jozsa, Phys. Rev. Lett. **74**, 4083 (1995).
[16] S. S. Hegde, J. Zhang, and D. Suter, Phys. Rev. Lett. **124**, 220501 (2020).
[17] T. H. Taminiau, J. J. T. Wagenaar, T. Van der Sar, F. Jelezko, V. V. Dobrovitski, and R. Hanson, Phys. Rev. Lett. **109**, 137602 (2012).
[18] N. Khaneja, T. Reiss, C. Kehlet, T. Schulte-Herbrüggen, and S. J. Glaser, J. Magn. Reson. **172**, 296 (2005).
[19] I. Lovchinsky, A. Sushkov, E. Urbach, N. P. de Leon, S. Choi, K. De Greve, R. Evans, R. Gertner, E. Bersin, C. Müller *et al.*, Science **351**, 836 (2016).
[20] S. Lloyd, Nature (London) **406**, 1047 (2000).

[21] I. Oliveira, R. Sarthour Jr, T. Bonagamba, E. Azevedo, and J. C. Freitas, *NMR Quantum Information Processing* (Elsevier, New York, 2011).
[22] A. Pati, S. Jain, A. Mitra, and R. Ramanna, Phys. Lett. A **301**, 125 (2002).
[23] J. Zhang, A. M. Souza, F. D. Brandao, and D. Suter, Phys. Rev. Lett. **112**, 050502 (2014).
[24] T. Van der Sar, Z. Wang, M. Blok, H. Bernien, T. Taminiau, D. Toyli, D. Lidar, D. Awschalom, R. Hanson, and V. Dobrovitski, Nature (London) **484**, 82 (2012).
[25] J. Zhang, S. S. Hegde, and D. Suter, Phys. Rev. Applied **12**, 064047 (2019).
[26] T. Gaebel, M. Domhan, I. Popa, C. Wittmann, P. Neumann, F. Jelezko, J. R. Rabeau, N. Stavrias, A. D. Greentree, S. Prawer *et al.*, Nat. Phys. **2**, 408 (2006).
[27] P. Neumann, N. Mizuochi, F. Rempp, P. Hemmer, H. Watanabe, S. Yamasaki, V. Jacques, T. Gaebel, F. Jelezko, and J. Wrachtrup, Science **320**, 1326 (2008).
[28] P. C. Maurer, G. Kucsko, C. Latta, L. Jiang, N. Y. Yao, S. D. Bennett, F. Pastawski, D. Hunger, N. Chisholm, M. Markham *et al.*, Science **336**, 1283 (2013).
[29] L. Childress, M. G. Dutt, J. Taylor, A. Zibrov, F. Jelezko, J. Wrachtrup, P. Hemmer, and M. Lukin, Science **314**, 281 (2006).
[30] D. Suter and F. Jelezko, Prog. Nucl. Magn. Reson. Spectrosc. **98**, 50 (2017).
[31] See Supplemental Material at http://link.aps.org/supplemental/10.1103/PhysRevLett.128.230502 for details on the Hamiltonian in the interaction frame, and clean-up operations U_{cu} and V_{cu}.
[32] J. Zhang, S. S. Hegde, and D. Suter, arXiv:2108.13738.
[33] J. Zhang, S. S. Hegde, and D. Suter, Phys. Rev. A **98**, 042302 (2018).
[34] N. Mizuochi, P. Neumann, F. Rempp, J. Beck, V. Jacques, P. Siyushev, K. Nakamura, D. J. Twitchen, H. Watanabe, S. Yamasaki, F. Jelezko, and J. Wrachtrup, Phys. Rev. B **80**, 041201 (2009).